ROCKET COMBUSTOR EXPERIMENTS AND ANALYSES

William E. Anderson, James C. Sisco, and In-Kyung Sung
School of Aeronautics and Astronautics
Purdue University
West Lafayette IN 47907

ABSTRACT

Results from laboratory-scale experiments and coupled analysis of rocket combustor energy release and life characterization are presented. The energy release is determined through axial pressure measurements and the one-dimensional compressible flow calculations. A model flow monopropellant was used in this preliminary exercise because of the simplifying approximations that could be employed and because the low enthalpy addition of the monopropellant reaction provides a severe case of the measurement technique. A liquid spray of hydrogen peroxide was injected into a stream of decomposed products, and axial pressure profiles and heat flux were measured. Constant gas properties were assumed in the one-dimensional model along with a D-squared drop vaporization submodel, but comparison of the model results with measurements show that a more accurate energy balance that includes heat transfer to the liquid phase is necessary. The life characterization work included a 'test-to-failure' of a laboratory combustor comprising a precombustor to generate hot gas and a water-cooled copper liner test section that was fitted into a stainless steel structural jacket. A thermal analysis of the liner was first validated using the measured coolant temperature rise. The life analyses were conducted with updated environments imposed on the liner. Both conventional (effective stress-strain) and advanced life prediction methods were used to predict between 50 and 320 life cycles. An unexpected type of failure occurred near the 100^{th} cycle, but a limited evaluation of the failed test article indicated that the viscoplastic modeling showed better agreement than conventional methods in predicting the life cycle failure when both low cycle fatigue and elevated temperature loads were applied. Improvements to the life prediction methodology are also discussed.

INTRODUCTION

The major requirements imposed on a rocket combustor are performance and life. Cost and reliability considerations are motivating the development of new designs using new materials in possibly new cycles. Although the aerospace community has typically relied heavily on derivative designs for new systems, limited design heritage exists for the propulsion systems that can meet these life and cost goals. Furthermore conducting a development program for large engines using full-scale hardware is prohibitive. Thus, the need for accurate design analysis models is more pressing than ever.

A need presently exists for an improved methodology to produce innovative designs and validation data for both first order and detailed design analysis early in the design cycle. Testing with subscale hardware is a valuable way to produce performance, heat transfer, life, and, in some cases, stability validation data. Smaller scale testing, on the single element level implies lower cost. A wider range of design and operating parameters can be examined. This paper describes work ongoing at Purdue

University to develop methodologies that combine laboratory-scale experiments with analysis for larger-scale design validation. Work related to injectors and chamber life is underway.

The injector effort seeks to develop a simple methodology that can be used to develop and assess injector designs using a one-dimensional combustion model, verify the one-dimensional model output with a simple high-pressure test device, and provide initialized combustor flowfield data for detailed CFD analysis of the injector concepts. The effort emphasizes the study of full-scale injector elements operated at realistic conditions. Key measurements in this approach include axial pressure profile and heat flux. In this paper a numerical model used to predict energy release profiles for correlation with measured axial pressure profiles is discussed. Validation case results are reported along with the actual case results. A limited number of differential pressure and heat flux measurements are reported and compared with the analytical results. .

The long-term goal of the chamber life effort described here is the development of a test-bed for the evaluation of long-life technologies including analytical approaches, innovative functional designs, advanced materials, and integrated health monitoring. The near-term goal of this work is to develop an integrated analytical/experimental approach for life prediction using prototypical subscale combustors. Results from a recent 'test-to-failure' experiment using a water-cooled copper liner at modest operating conditions are provided. The liner was designed to fail in a verifiable number of cycles using different analytical methods. Although the liner failed in an unexpected mode, valuable lessons were learned regarding the further development of the approach.

The experimental and analytical approaches used in both areas are described in this paper. Shortcomings in the present application of each approach were discovered and plans to improve each are discussed.

COMBUSTION CHARACTERIZATION

This combined experimental/analytical approach described below was demonstrated earlier by Bracco and others[1,2,3,4] using liquid oxygen and hydrocarbon propellants. In the present work, liquid hydrogen peroxide (HP) is injected into a decomposed stream of HP. Mass and enthalpy addition profiles are determined by the measurement of axial pressure profile and heat flux measurements in a modular chamber. The use of the HP monopropellant provides the advantage of a vaporizing and reacting gas flow with the approximation of constant gas properties. It also provides a relatively severe test of the measurement approach because the pressure loss due to mass and enthalpy addition is much lower than in a bipropellant case, which is the eventual application. This approach is particularly useful for characterizing full-scale injector element designs at realistic operating conditions.

EXPERIMENTAL APPROACH

Experiments were conducted at Test Cell A of Advanced Propellants and Combustion Laboratory (APCL) in Purdue University. A detailed description of the test facility and data acquisition is described elsewhere.[5] The test facility is capable of handling separate flow systems for both oxidizer and fuel. For

the HP decomposition studies, two separate oxidizer tanks were used allowing us to vary the concentration of liquid HP injected downstream of the decomposed hot gas stream of HP.

A flow of HP decomposed in a catalyst bed made provided the main (primary) hot gas stream. Three four-inch long and one two-inch long cylindrical chambers with an inside diameter of 1.2 in were built from copper rod stock. All chambers were equipped with axial pressure ports for differential pressure transducers. Also, two four-inch chambers were furnished with ports for heat flux gauges. In addition to the differential pressure ports, absolute pressure and thermocouple ports were made in all the chamber sections. Four throat sections allowing contraction ratios of 4.9, 5.7, 6.7, and 8.0 were made of stainless steel.

Measurements of axial pressure along the chamber were made using highly accurate differential pressure transducers. Two different ranges of differential pressure transducers, 50 psid and 250 psid, were used. The accuracies of the differential pressure transducers were 0.04% and 0.25% of the full scale, respectively. Chamber pressure was recorded using standard absolute pressure transducer with 0.25% accuracy of the full scale. Two Gardon-type heat flux gauges with ratings of 1000 Btu/ft^2-s and 2000 Btu/ft^2-s were used to measure heat flux. Temperature measurements were made using six-inch long K-type thermocouples with maximum temperature rating of 2500 ºF. Figure 1 is a dimensioned line drawing showing the instrumentation locations.

During preliminary tests, pressure surges during the startup and shutdown transients exceeded the differential pressure range of the differential pressure transducers. The surges were sufficiently large that two out of three transducers with a 50 psid range were destroyed. A variety of methods were investigated to eliminate the differential surges, including using snubbers, purging the instrumentation lines, and using lines of different internal diameters and lengths. The line purge reduced the magnitude of the pressure spike, but it introduced hysteresis effects that prevented the acquisition of accurate and repeatable measurements. Finally differential pressure transducers with large ranges (250 psid) were used. This solved the problem of damaging the transducers, but at a loss of accuracy.

ANALYTICAL APPROACH

The model is based on the generalized one-dimensional equations[6] which typically take into account the physical effects of area change; wall friction; external heat transfer; chemical reaction; change of phase; and changes in molecular weight and specific heat. The study fluid is hydrogen peroxide. The use of a monopropellant allowed the approximate simplifying assumption of constant gas properties, although we will show later that this approximation leads to major differences with the measurements. Also, the bi-component drop is assumed to vaporize uniformly, and vapor phase decomposition kinetics are assumed to be infinitely fast. Enthalpy addition occurs simultaneously with mass addition, without gas property change.

There are eight basic and governing equations for the generalized one-dimensional compressible flow, which have fourteen differential variables. Some of these variables can be easily set to zero due to the approximations set forth in our application of this model. The equations are expressed in logarithmic differential form to allow easy separation of the physical effects mentioned above. Among the fourteen

differential variables, six variables may be chosen as independent variables and eight as dependent variables. The independent variables are the *influence coefficients*, which can be controlled most easily in practice.

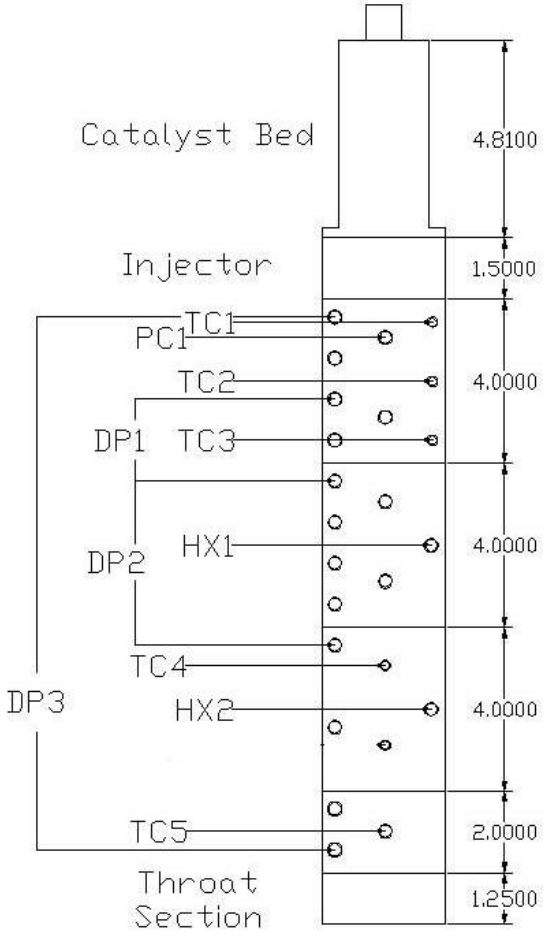

Figure 1: The 14-inch long configuration with the locations of instrumentation. DP indicates differential pressure measurements. HX indicates heat flux measurements. Dimensions are in inches.

For this model, the most important dependent variables are Mach number and pressure. Mach number can be written in differential form as

$$\frac{dM^2}{M^2} = \frac{-2\left(1+\frac{k-1}{2}M^2\right)}{1-M^2}\frac{dA}{A} + \frac{1+kM^2}{1-M^2}\frac{dQ+dH}{C_p T} + kM^2\frac{\left(1+\frac{k-1}{2}M^2\right)}{1-M^2}4f\frac{dx}{D} + \frac{2\left(1+kM^2\right)\left(1+\frac{k-1}{2}M^2\right)}{1-M^2}\frac{d\dot{m}}{\dot{m}} \qquad (1)$$

Solving for pressure yields

$$\frac{dP}{P} = \frac{kM^2}{1-M^2}\frac{dA}{A} - \frac{kM^2}{1-M^2}\frac{dQ + dH}{C_p T} - \frac{kM^2(1+(k-1)M^2)}{2(1-M^2)} 4 f \frac{dx}{D} - \frac{2kM^2\left(1+\frac{k-1}{2}M^2\right)}{1-M^2}\frac{d\dot{m}}{\dot{m}} \quad (2)$$

For the one-dimensional model as used here, only the influence coefficients of enthalpy, mass addition, friction, and heat transfer are considered. The influence coefficient for the frictional loss was evaluated using the friction factor[7]

$$f = \frac{0.25/4}{\left[\log\left(\frac{e}{3.7D} + \frac{5.74}{\mathrm{Re}_D^{0.9}}\right)\right]^2} \quad (3)$$

Heat transfer was calculated by assuming that convective heat transfer dominates

$$Q = h_g A(T - Tw) \quad (4)$$

and the convective heat transfer coefficient was calculated using the empirical Bartz correlation

$$h_g = \left[\frac{0.026}{D_t^{0.2}}\left(\frac{m^{0.2} C_p}{\mathrm{Pr}^{0.6}}\right)_c \left(\frac{P_C g}{C^*}\right)^{0.8}\left(\frac{D_t}{R}\right)^{0.1}\right]\left(\frac{At}{A}\right)^{0.9} s \quad (5)$$

where s is the correction factor which is assumed to be unity for these calculations. Furthermore, the gas temperature is assumed to be constant in the chamber. Both a constant wall temperature and an adiabatic wall condition were assumed; these assumptions will be discussed later. Therefore, only the heat transfer coefficient varies along the axial location. To calculate the heat loss, the heat transfer rate for the constant wall temperature assumption was integrated over the surface area of the chamber.

The enthalpy and mass addition were calculated in the vaporization model. These two influence coefficients are coupled and cannot be treated separately. A simple vaporization model was implemented to evaluate these parameters using the classic D^2-Law[8] with the assumption of a monodisperse drop distribution:

$$\frac{dD^2}{dt} = -\frac{8k_g}{r_l C_{pg}}\ln(B_q + 1) \quad (6)$$

where the right-hand side of the equation is also called as evaporation constant K. The equation (6) is written is function of time, and can be converted as function of axial distance of the chamber using the following equation

$$\frac{dD^2}{dx} = \frac{1}{V_d}\frac{dD^2}{dt} \quad (7)$$

Finally, the evaporation constant evaluated in the equation (7) is based on the condition of burning drops at a stagnant medium. Therefore, the value of K must be corrected to the forced-convection environment as shown below,

$$K = K^\circ(1 + 0.276\ \mathrm{Re}^{1/2}\ \mathrm{Pr}^{1/3}) \quad (8)$$

The initial drop diameter is computed based on an empirical correlation for the crossflow injector. A number of correlations exist, but the one that was developed from conditions most closely matching the experimental conditions was[9]

$$Do = 3.9\,Din\left(\frac{1}{We\ \mathrm{Re}}\right)^{0.25} \qquad (9)$$

The empirical correction factor of 3.9 in Equation (9) was varied in the model to provide a match with the measured characteristic exhaust velocity efficiency.

The one-dimensional model was written in Matlab script. The initial and boundary conditions were set based on each test condition along with chemical equilibrium code results. All necessary influence coefficients along the axial position of the chamber were known values. A fourth order Runge-Kutta method was implemented. An iterative solution was used based on matching the gas density at the sonic throat. Validation of the numerical model was done by separate comparisons with analytical solutions of isentropic flow with area change, Rayleigh flow, and Fanno flow. A numerical discretization of 400 points gave satisfactory accuracy.

An illustration of the numerical model results is shown in Figure 2. The results are for the case where it is stipulated that the axial location for complete reaction of the injected hydrogen peroxide is the throat. For the sample calculation, the initial drop size was iterated on until the liquid flow was completely vaporized exactly at 14 in. An adiabatic wall condition was assumed along with 100% efficiency of the catalyst bed flow. Infinitely fast vapor phase decomposition kinetics were also assumed. Also shown in the figure are the locations of the three differential pressure measurements DP1, DP2, and DP3. The pressure drops due to friction, enthalpy addition, and mass addition were 0.3, 4.1, and 12.1 psid, respectively, with a total pressure drop of 16.5 psid.

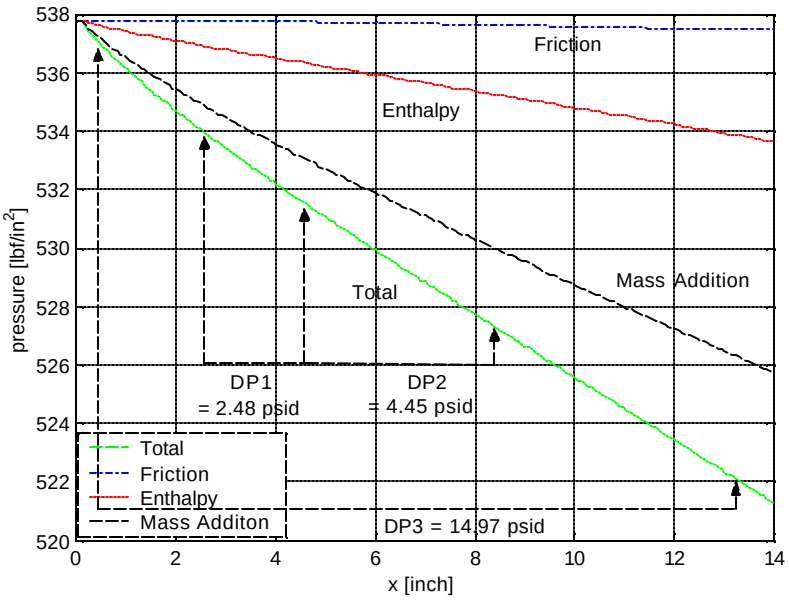

Figure 2: One-dimensional model results.

The numerical analysis includes a submodel for pressure loss due to heat transfer. In the experiments, the heat loss is from the gas to the cooler chamber, and from the gas to the evaporating drops, thus a pressure rise would be calculated. The major uncertainty in the chamber wall heat loss model is the hot side wall temperature, which changes during the course of a test. Gardon-type heat flux gauges were installed at two locations in the chamber. The most repeatable heat flux measurement indicated heat flux levels close to 1.0 Btu/in^2-s. To evaluate the use of the heat loss model, the numerical results of Figure 2 were compared with a case where the heat flux was twice that of the measured value. The difference in pressure drop for the two cases was 0.4 psi, representing about a 2.5 percent difference. Because of the small relative difference in calculated pressure drop, and the uncertainty in specifying a hot-side-wall temperature for the heat flux calculation, an adiabatic wall approximation was used in subsequent calculations.

RESULTS

Since a high gas velocity (low chamber contraction ratio) tends to increases the pressure gradients, a low contraction ratio of 4.9 was chosen for the experiments discussed below. A test matrix (see Table 3) was devised which varied the mass split between primary gas flow secondary liquid flow was varied from 90/10 to 70/30. Three differential pressure measurements (DP1-3) and one heat flux measurement (HX2) were obtained as shown in Figure 1.

During Test Nos. 1 through 3, instrumentation line purges were used to reduce the pressure spiking during startup and shutdown as discussed in the Experimental Approach section. Although the line purges provided some damping, they also apparently caused hysteresis effects, resulting in a zero-shift in the pressure measurement after the first test. The reliability of the measurement was therefore brought into question, and the line purges were eliminated. The low range pressure differential transducers were removed and only the high range (250 psid range) transducers were used. Only Test Nos. 4 and 5 will therefore be discussed here.

Table 1: Experimental Test Matrix for Differential Pressure and Heat Flux Measurement.

Mass Split (G/L)	Test No	Lc In.	CR	Injector Type	Venturi D. In.	mdot_M lbm/sec	mdot_S lbm/sec	Mono_Pc psi	Pc psi
90/10	01	14	4.90	A	0.078/0.030	0.900	0.100	376.35	418.16
70/30	02	14	4.90	A	0.078/0.054B	0.900	0.386	376.35	537.76
70/30	03	14	4.90	A	0.078/0.054B	0.900	0.386	376.35	537.76
80/20	04	14	4.90	A	0.054A/0.030	0.450	0.113	188.17	235.42
80/20	05	14	4.90	A	0.068/0.034	0.700	0.175	292.71	365.89

Another experimental difficulty arose at the start of this test series. The decomposition efficiency of the catalyst bed dropped from the earlier values of more than 90% to around 70%. This catalyst bed served as a workhorse gas generator in our laboratory and is probably approaching the limit of its useful

life. Thus the approximation that the temperature of the primary gas flow was the decomposition temperature of hydrogen peroxide was no longer valid.
Test No. 4 was added to the matrix to reduce the flow through the catalyst bed to achieve higher decomposition efficiencies as well as to evaluate the pressure spikes at a presumably safer low flow condition. Although the low primary flow rates resulted in higher decomposition efficiency approaching 0.9, the low secondary flow rates resulted in poor atomization of the liquid peroxide due to the low liquid injection pressure drop and thus poor secondary flow decomposition efficiencies. Heat flux measurements were repeatable though and results from heat transfer gauge HX2 are shown in Figure 3.

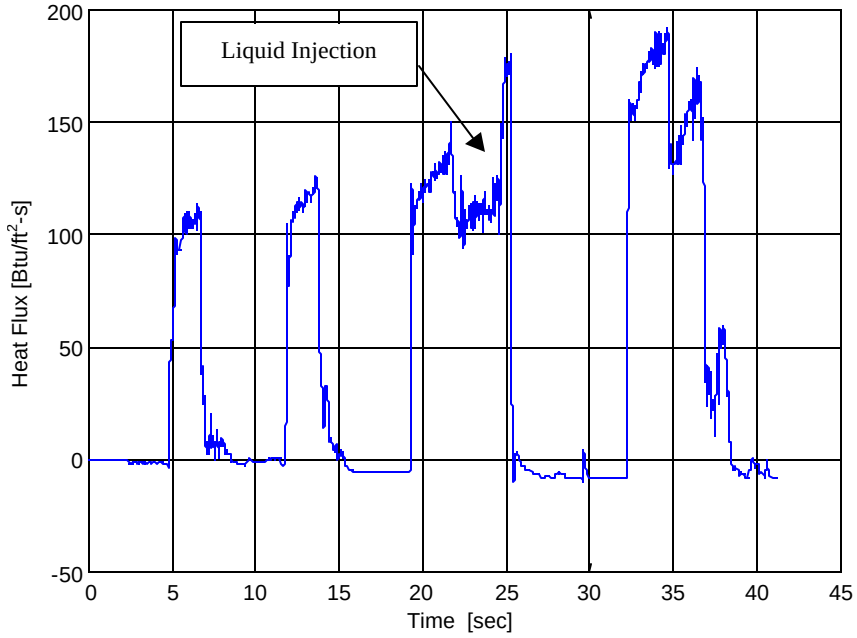

Figure 3: Heat flux measurement at HX2 (see Figure 1) for Test No. 4.

The C* efficiency of the primary flow prior to the injection of liquid flow was only about 70% for Test No. 5. The measured pressure gradients are shown in Figure 5. The DP1 measurement near the front end of the chamber indicated a pressure rise near zero at the initiation of secondary flow and approaching 0.5 psi near the end of the test, a trend that was also seen in Test No. 4. The DP2 and DP3 measurements both indicated pressure drops of about 1.2 and 0.5 psi, respectively. Again these trends were also evident in Test No. 4.

The numerical model was exercised for Test Nos. 4 and 5. The model was forced to match the experimental data by adjusting the initial drop size until the calculated value of static chamber pressure matched the measured value. Effective mass addition is defined here by the amount of mass that must be added to the decomposed primary flow to achieve the measured chamber pressure. The decomposed primary flow was determined from the chamber pressure measurement prior to secondary liquid injection. The effective mass addition for Test No. 4, plotted as a function of chamber length in Figure 6, was thus determined to be 36.6% of the injected liquid flow rate. The pressure drop across the entire length of the chamber due to this mass addition was 80% of the total pressure drop.

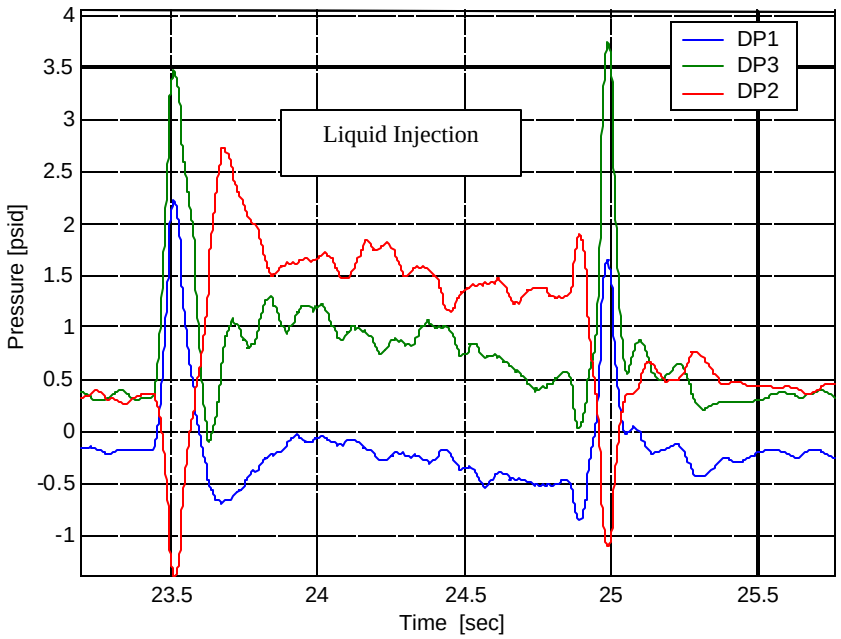

Figure 4: Differential pressure measurement for Test No. 5. A two-Hz filter is used.

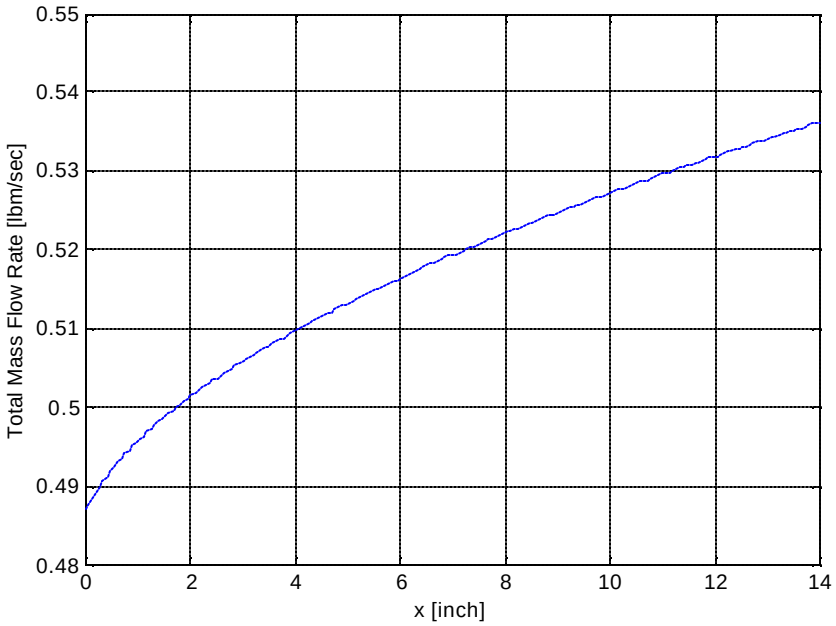

Figure 6: Calculated mass addition profile for Test No. 4. Overall mass addition was set by stipulating the chamber end pressure to be equal to the measured pressure.

Figure 7 illustrates both numerical and experimental results for Test No. 4. The numerical result is plotted as a continuous pressure profile. The DP measurements are shown as points at the axial location of their downstream measurement. The upstream reference point for the DP data in the figure is the calculated pressure at the axial location of the upstream measurement. As mentioned earlier, these results are not what were expected. We expected a monotonic pressure drop indicating relatively steady mass and enthalpy addition. Certainly the unfortunate reduction of the catalyst bed efficiency contributes to some of the difficulty in data interpretation. However an explanation may also lie in our analysis of the drop vaporization and the approximation of constant gas properties.

Our use of the D^2-Law did not account for the energy transport between the decomposed gas and the liquid drops, a simplification which is of course inconsistent with the realistic condition. As the drops heat up to the saturation temperature, heat will be lost from the gas to the drops. The pressure rise indicated by the DP1 measurements could actually be due to an initial drop heating period and evaporation, resulting in a heat loss from the gas and thus in a pressure rise. An estimate of the pressure rise due to the drop heating and evaporative cooling was made and is about 0.4 psid for Test No. 5. In the section of the chamber measured by DP2, vaporization and decomposition of the heated secondary injected flow could be occurring, resulting in a higher pressure drop than predicted. Because the upstream port of DP3 is in the imagined "drop heating" regime, and the downstream port of DP3 is in the imagined "vaporizing" regime, the pressure drop indicated by DP3 would be less than that measured by DP2. The fact that DP3 is about equal to the sum of DP1 and DP2 further substantiates this explanation. Other contributing factors could include finite decomposition kinetics, and of course the inefficient catalyst bed is a complication. The inclusion of a more accurate submodel for energy transport between the gas and liquid phase, an analysis of vapor phase kinetics, and a modification to the catalyst bed to provide near 100% decomposition of the primary flow are all presently underway.

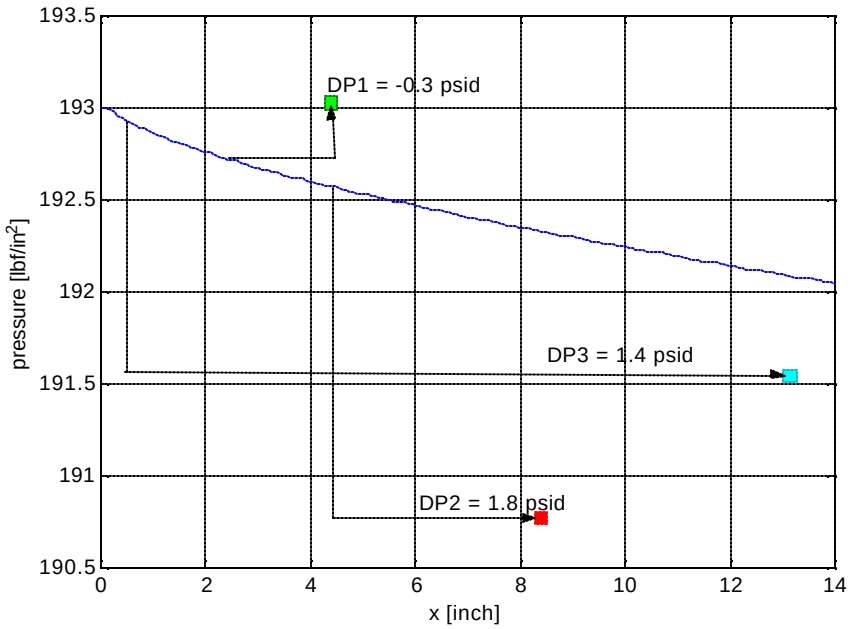

Figure 7: Pressure Profile for Test No. 4 with experimental data.

LIFE CHARACTERIZATION

The long-term goal of this study is to develop a combined experimental./analytical approach that uses subscale prototype hardware to determine likely failure modes and obtain model validation data. The specific objectives of the present study were three-fold: to qualitatively predict the expected failure mechanism of the gradual thinning of the cooling passage and the so-called "dog house" effect by using a visco-plastic model; to verify theoretical life estimation by using test data; and to provide students in the School of Aeronautics and Astronautics at Purdue with the experience of a "design, build, and test" rocket engine combustor project. First a brief review of previous work in life prediction is presented, with an emphasis on studies that used subscale test hardware. An analysis based on the viscoplastic treatment of stress and strain is then presented. Then the experimental hardware is described along with the test approach used in this study. Finally the results are discussed and compared to the analytical predictions.

ANALYTICAL APPROACH

The method developed by Dai and Ray[10] is based on the concepts of sandwich beam model and viscoplasticity to represent progressive bulging and thinning phenomena in the coolant channel of rocket engine. The total strain rate is the sum of elastic and inelastic strain:

$$e_{ij} = e_{ij}^{e} + e_{ij}^{in} \tag{10}$$

Each strain can be obtained by the integration of the elastic and inelastic strain rate:

$$\dot{e}_{ij}^{e} = \frac{(1+n)}{E}\dot{s}_{ij} - \frac{n}{E}\dot{s}_{kk}d_{ij} \tag{11}$$

$$\dot{e}_{ij}^{th} = a\dot{T} \tag{12}$$

To compute the inelastic strain rate the Freed viscoplastic model[11] was introduced. From the inelastic strain, the pressure distribution and the geometric configuration of the cooling channel, the time-dependent radial deflection at the midplane of the hot wall can be obtained:

$$\begin{aligned} w(x,t) = {} & \frac{\tilde{C}x^2 p(t)}{6}\left(\ell^2 - \ell x + \frac{x^2}{4}\right) \\ & + \frac{1}{d_1 + d_2}\left(\frac{x^2}{2\ell}\int_0^{\ell}\tilde{I}_2^{in}dx - \int_0^{x}\int_0^{h}\tilde{I}_2^{in}dxdh\right) \end{aligned} \tag{13}$$

where subscripts 1 and 2 denote coolant and hot side thin faces of the sandwich beam model, respectively, and where $\tilde{C} = \dfrac{A_1E_1 + A_2E_2}{A_1A_2E_1E_2(d_1+d_2)^2}$, $\tilde{I}_2^{in} = e_2^{in} - e_1^{in}$, p(t) = distributed force per unit

length, l = half length of the ligament, x = ligament width, A_1, A_2 = cross section area of sandwich beam 1 and 2, E_1, E_2 = Young's modulus of face 1 and 2, and d_1, d_2 = distance between the thin faces.

The first term on the right hand side of Eq. (13) shows the reversible components of the radial deflection and the second term represents the permanent bulging and progressive thinning of the coolant channel wall. With this radial deflection w(t) at the midplane of the ligament, the normalized thinning rate is expressed as:

$$\bar{t}(t) = \frac{\left(\frac{4\ell}{a}+1\right)w(t)}{\frac{4\ell}{a}\left(\frac{2\ell}{a}+1\right)J_0} \qquad (14)$$

where a is the distance between channels and ?$_0$ is the original ligament thickness

Finally life was computed as:

$$Life = \frac{q_0 - q_{cr}}{\bar{t}(t)} \qquad (15)$$

and critical thickness by:

$$q_{cr} = q_0 \exp(-q) \qquad (16)$$

Where $q = 0.2[(S_u-S_y)/S_y]^{0.6}$, S_u = ultimate stress, and S_y = yield stress. Freed's phenomenological viscoplastic model was used to determine properties for the ductile material over a wide range of temperatures. The material constants can be obtained from isothermal experiment data.[11]

EXPERIMENTAL APPROACH

A small scale combustion chamber was designed, built and tested by senior and first year graduate level students in the School of Aeronautics and Astronautics at Purdue University. The students derived specific design requirements from the following top-level requirements:

- a low cycle fatigue failure mechanism had to be demonstrated within a reasonable number of cycles (<200);
- the experiment had to verify a life prediction analysis from conventional modeling approaches;
- the environments in the test section had to be well-characterized and results from the thermal analysis had to be verifiable;
- the water cooled liner could not melt prior to the LCF failure;
- conventional design analysis methods were used;
- all parts had to be manufactured in the Aerospace Sciences Laboratory at Purdue.

The main components of the test article (Figure 8, from top to bottom) were a catalyst bed to decompose 90% by weight hydrogen peroxide, a fuel injector, a copper heat sink precombustor with sufficient volume to provide complete combustion and mixing of the decomposed oxidizer and fuel, and the test section, which comprised a plug nozzle and a water-cooled oxygen-free high-conductivity (CU102) copper liner. This configuration is similar to that used at NASA Lewis Research Center.[12,13] Design and operating parameters are given in Table 2.

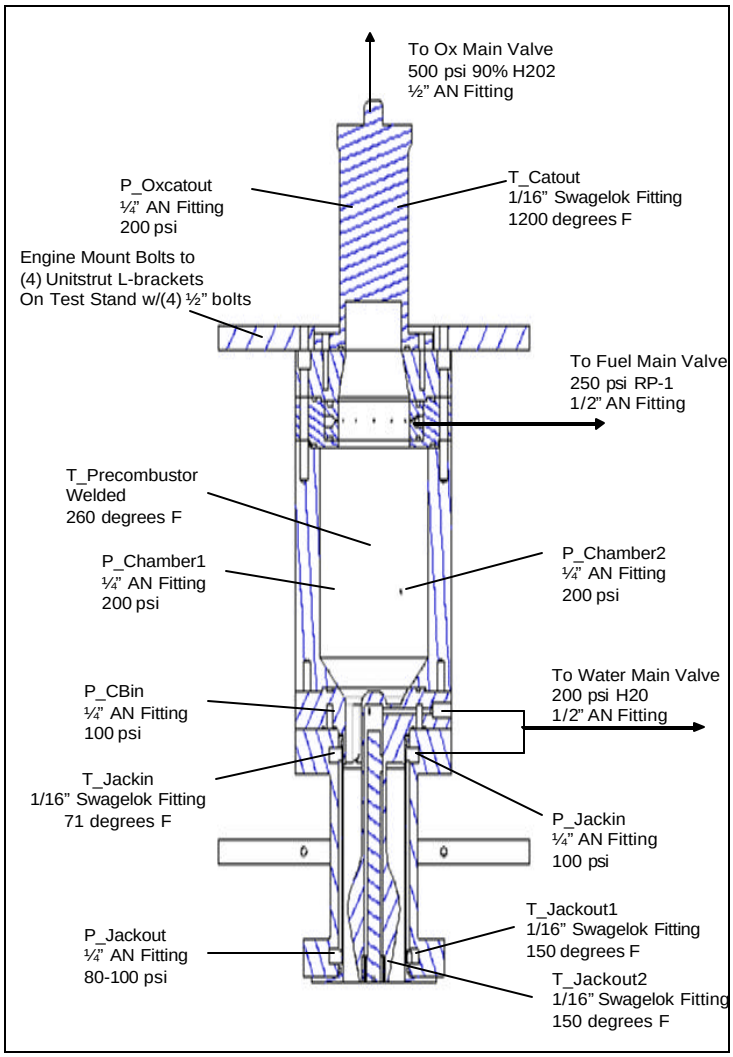

Figure 8: Test article schematic and interfaces. A catalyst bed is used to decompose hydrogen peroxide, which is then sent to the precombustor to burn with JP-8 to produce a well-mixed hot gas. The hot gas enters the test section composed of the water-cooled liner and centerbody. The throat of the test section is formed by the diverging centerbody.

Table 2: Operating and Design Parameters

Parameter	Value
Propellant Mixture Ratio (O/F)	4.0
Oxidizer Mass Flow Rate	1.0 lb/s
Fuel Mass Flow Rate	0.25 lb/s
Chamber Pressure (P_c)	200 psia
Characteristic Velocity (C^*)	4961 ft/s
Specific Impulse (I_{sp})	205.1 s
Chamber Temperature (T_c)	3900 °R
Expansion Ratio (ε)	2.8
Nozzle Throat Area (A_t)	0.915 in^2
Nozzle Exit Area (A_e)	2.56 in^2
Nozzle Throat Diameter (D_t)	1.08 in
Chamber Diameter (D_c)	3.5 in
Contraction Ratio (CR)	10.5
Characteristic Length (L^*)	70
Chamber Volume (V_c)	64 in^3
Chamber Length (L_c)	6.0 in
Injector Diameter (D_{in})	2.30 in
Number of Injector Holes	12
Injector Hole Diameter ($D_{in,h}$)	0.032 in

The cooled liner channel geometry was based on standard channel wall designs. The hot wall thickness was set at 0.030 in (which is within the design range for typical designs as well as being machinable in the Aerospace Sciences Laboratory machine shop) and the land width was set at 0.103 in. The channel width was 0.125 in and the channel height was 0.06 in. These channel geometries were determined to result in a failure within a reasonable number of cycles at the available combustor conditions.

A simple one-dimensional code using the Bartz and Seider-Tate equations[14] for hot- and coolant-side heat transfer coefficients, respectively, was developed and applied. The coolant flow rate was set to maintain a safe margin from a calculated burnout heat flux of **6.54** Btu/in^2-s. De-ionized water was used as coolant for both the center body and the chamber liner, which was dumped into the plume. Figure 9 shows the predicted wall temperatures along the chamber and nozzle. Detailed analysis of the temperature, stress, and strain field around the cooling channel was done using finite element analysis codes, namely ABAQUS and ANSYS.

Figures 10-12 show the assembly upstream of the nozzle, the water-cooled chamber liner and the water-cooled center-body. The chamber liner was designed to fit tightly within a stainless steel combustor case (not shown). The center-body was coated with thermal barrier coating (TBC). To avoid cracks due to differential thermal expansion, an aluminum/bronze bond layer was applied between the copper and the Rokide, a Zirconium Oxide TBC. Rokide is made up of 95% copper and 5% aluminum and was applied to a thickness of 0.01 in. After 140 firings, the coating was still intact at the throat of the center-body.

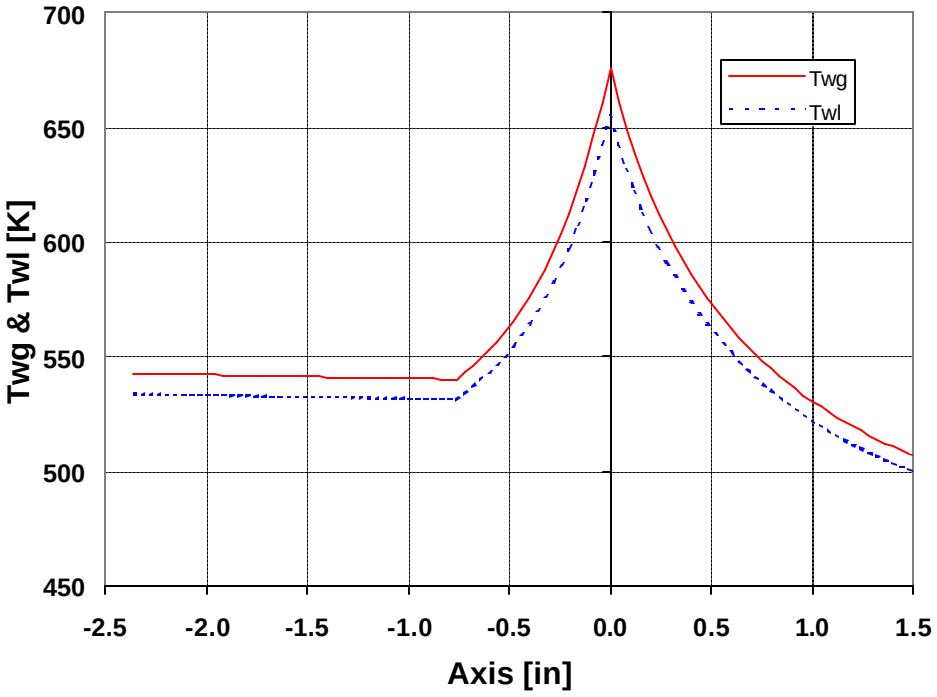

Figure 9: Predicted gas-side and coolant-side wall temperature as function of test section length. Throat is at 0.0 location.

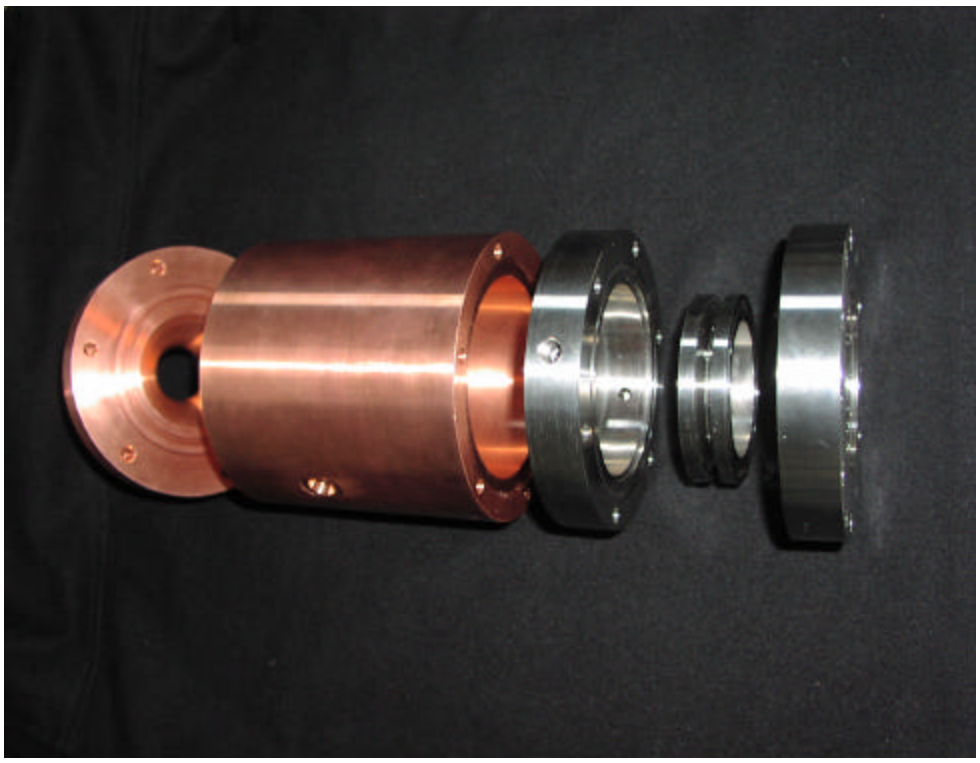

Figure 10: Assembly of injector and pre-combustor with a test nozzle.

Figure 11: Chamber liner before testing.

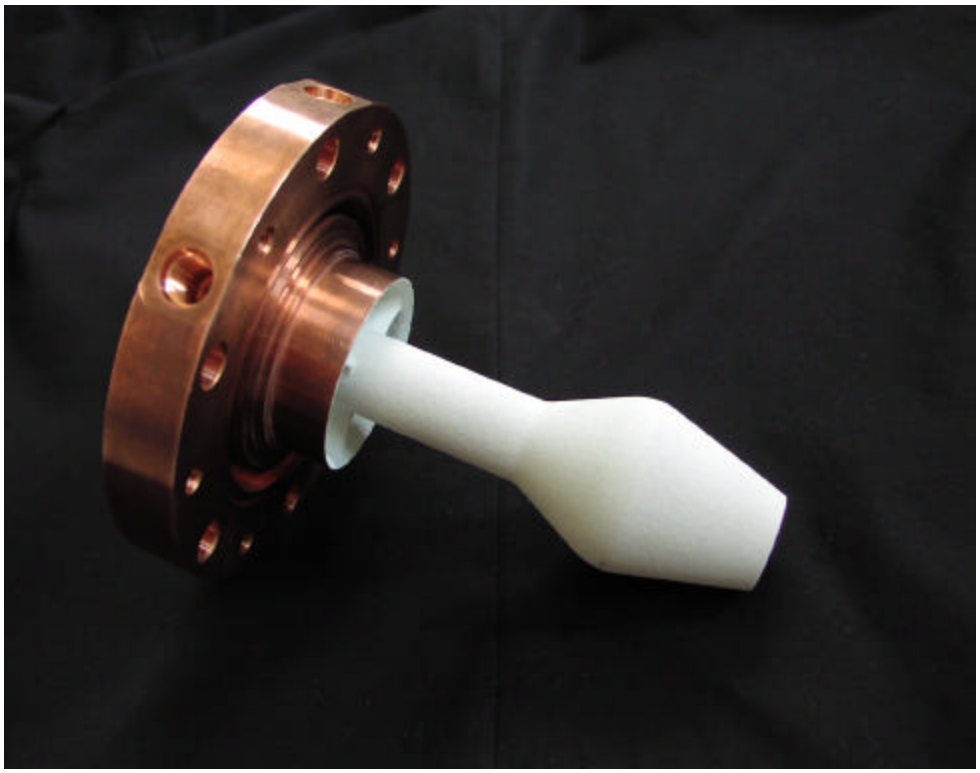

Figure 12: Center-body after TBC coating.

Testing was conducted in the Advanced Propellant and Combustion Laboratory (APCL) at Purdue University (http://engr.purdue.edu/AAE/Research/Propulsion/Facilities/apcl). The project took advantage of the major hardware previously installed in the test cell. Modifications were made to accommodate the requirements of this project. For instance, a 650 psia water tank was installed to provide water to both the center-body and the cooling liner. The flow timing sequence was automatically controlled with LABVIEW (National Instruments), which controlled the pneumatically actuated valves and the data acquisition system.

On average each cycle comprised a 0.5 s H_2O_2 lead, with a 1.0 s bipropellant (both fuel and oxidizer) firing, a 1.5 s H_2O_2 lag, and then a 2.0 s pause to allow the cooling channels to return to their initial temperatures. The lead and lag time were implemented to insure complete H_2O_2 decomposition and to burn any residual fuel left in the engine. This cycle was repeated (on average) twelve times for every test. Cooling water was flowed continuously throughout the cyclic testing.

Figure 13 shows chamber pressure typical of a series of cycles. The five pulses shown at the beginning of the test were monopropellant cycles used to raise the temperature of the catalyst bed prior to the bipropellant tests to ensure that the oxidizer was completely decomposed before it entered the precombustor. The C* efficiency of the precombustor was measured indicating that nearly complete combustion was occurring in the precombustor and that the gas environment in the test section could be closely characterized by one-dimensional equilibrium calculations. Figure 14 shows the measured coolant temperatures at the inlet and the outlet water ports. These measurements were the primary means used to verify the thermal analysis, which served as a basis for the life prediction analysis described later.

The rocket was disassembled after every ten or so cycles depending on the amount of propellant loaded. The cooling jacket was then visually inspected as well as dye-penetrant inspected. Notes were taken and pictures were taken to document the condition of the hardware.

RESULTS

A detailed finite element analysis was performed after the first set of data was obtained to provide verification data for the thermal analysis. Data reduction was performed by a MATLAB code written by the students. For verification of the thermal analysis results, the temperature rise of the coolant was measured. Figure 15 shows that the temperature rise predicted initially was somewhat lower than that which was measured. To determine actual liner conditions for input to the life analysis, the coolant temperature variation was corrected on the basis of the coolant temperature measurements.

Thermal and mechanical stress and strain were then computed using the corrected wall temperature values that were derived from the coolant water temperature measurements. To further verify the analytical values more detailed analyses using ANSYS and ABAQUS were used. Figure 16 shows the predicted temperature distribution in the wall at the throat region, indicating a maximum temperature of 714 K (825 F) and a temperature gradient of 1920 F/in.

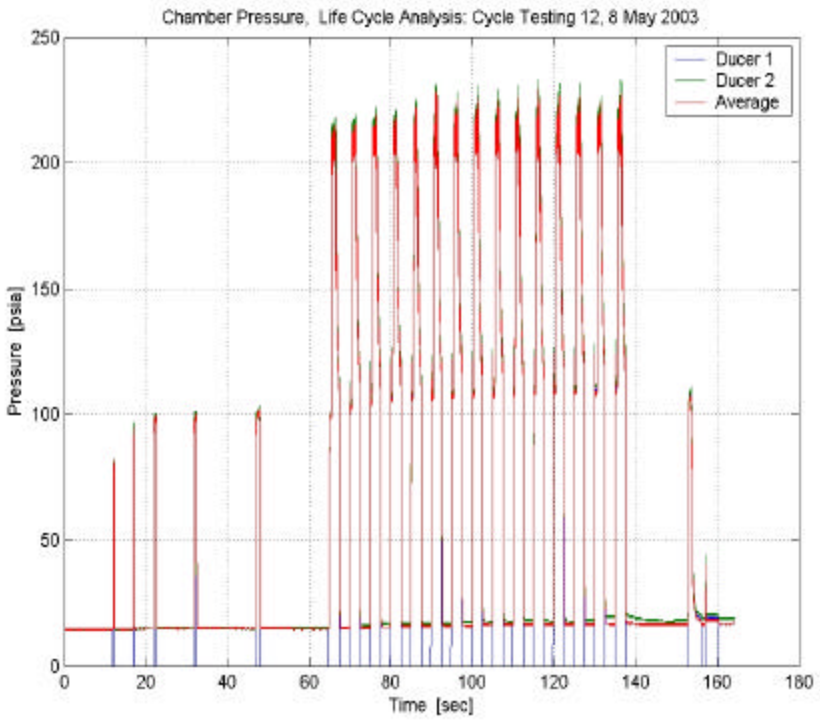

Figure 13: Experimental chamber pressure during cyclic testing.

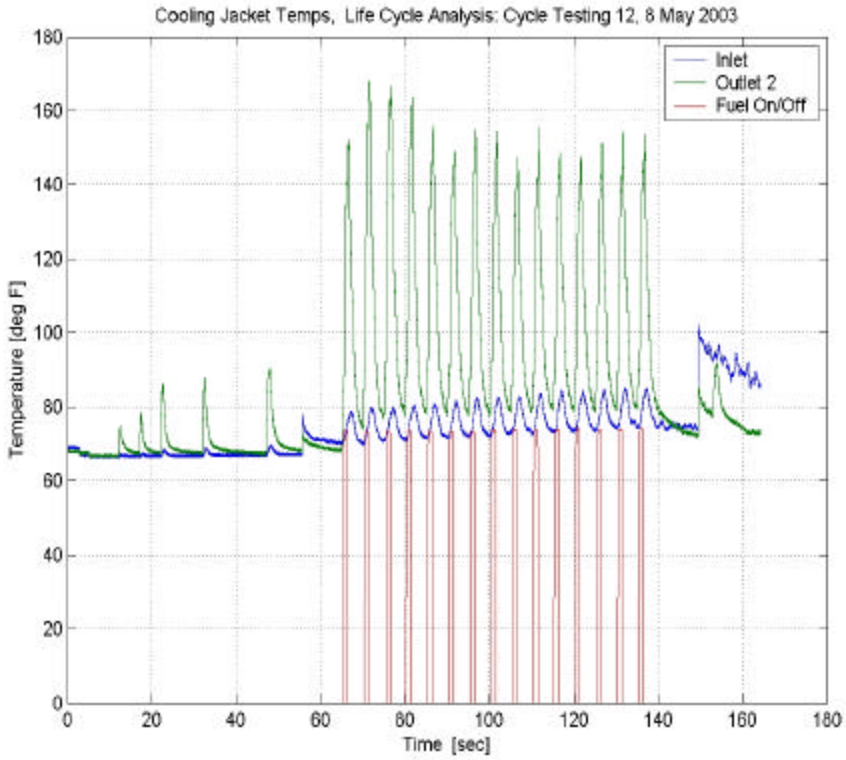

Figure 14: Coolant temperature during cyclic testing.

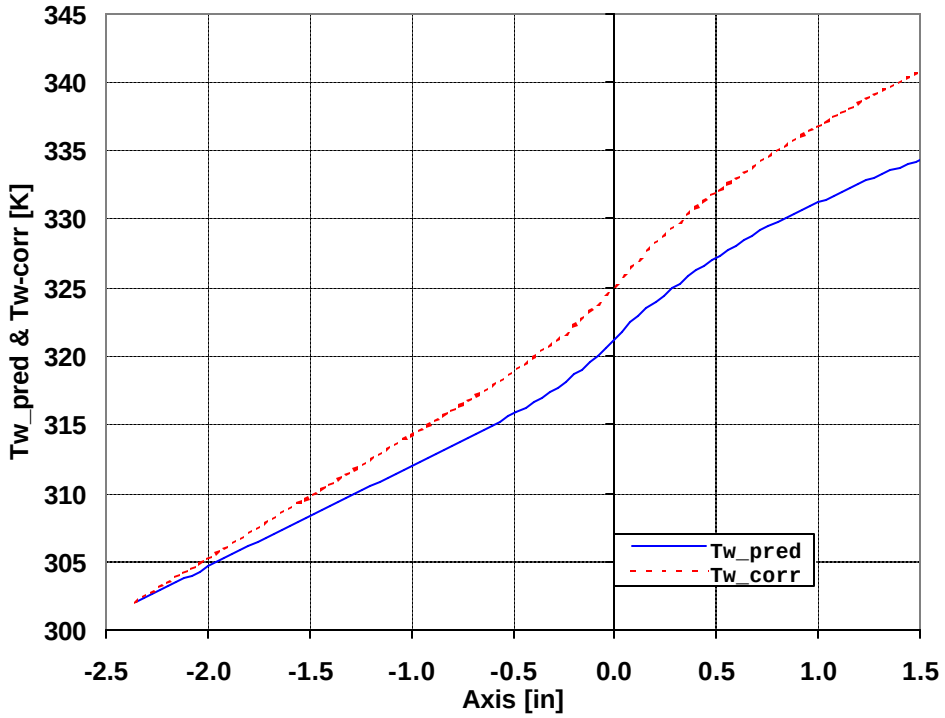

Figure 15: Predicted and measured coolant temperature as a function of channel length.

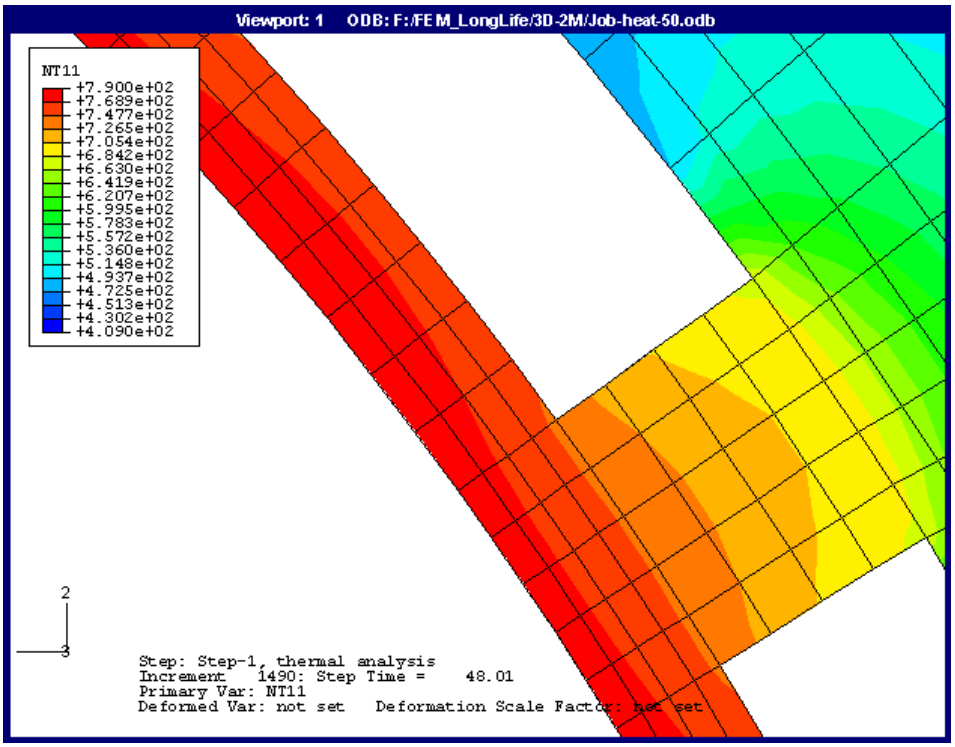

Figure 16: Wall temperature distribution around rectangular cooling channel. Maximum temperature (790 K) was occurred at the middle of the ligament.

From the calculated temperature distribution and pressure loading, the thermo-mechanical stress and strain were obtained. Figure 17 depicts total strain for the throat region at steady state conditions as computed by ANSYS. The maximum strains computed analytically and the ANSYS prediction were in agreement at about 2.0%. From the strain life (S-N) curve of OFHC,[15] Figure 18, the number of cycles to failure was predicted to be 115 cycles.

The method of Porowski[16] and the viscoplastic method estimated life to be between 51 and 260 cycles. A deformation in the throat region was noted at approximately the 90th cycle. To validate the viscoplastic prediction method, the nozzle test section deformation was measured. The thickness of the throat section that did not show deformation was partially increased. The original thickness of the throat was 0.030 in. The average thickness of the throat section where it was not deformed was changed to 0.032" after 140 cycles. The thickness of the deformed region was 0.029 in, so the reduced thickness was 0.003 in. Therefore, the thinning rate was calculated as 0.003 in/140 = 2.5E-5 in/cycle. The critical wall thickness, beyond which the crack growth rate became infinity, was computed to be 0.0242" by Eq. (16). The cycles to failure can be calculated using Eq. (15). Finally life was determined to be 270 cycles, which shows good agreement with the visco-plastic estimation.

Figure 19 shows the equivalent plastic strain. Since ABAQUS starts zero strain at the yield point, the total strain (1.2%) is the sum of plastic (1.0%) and elastic strain (0.2%). Total strain gives a life of 320 cycles from Figure 18. To see the progressive deformation and thinning of the wall, the throat region was modeled via ABAQUS and cyclic loading was applied up to 100 times, based on the loading history that was used. Figure 20 shows the deformation of the wall at 40 cycles, showing no deformation, and at 100 cycles, showing significant deformation.

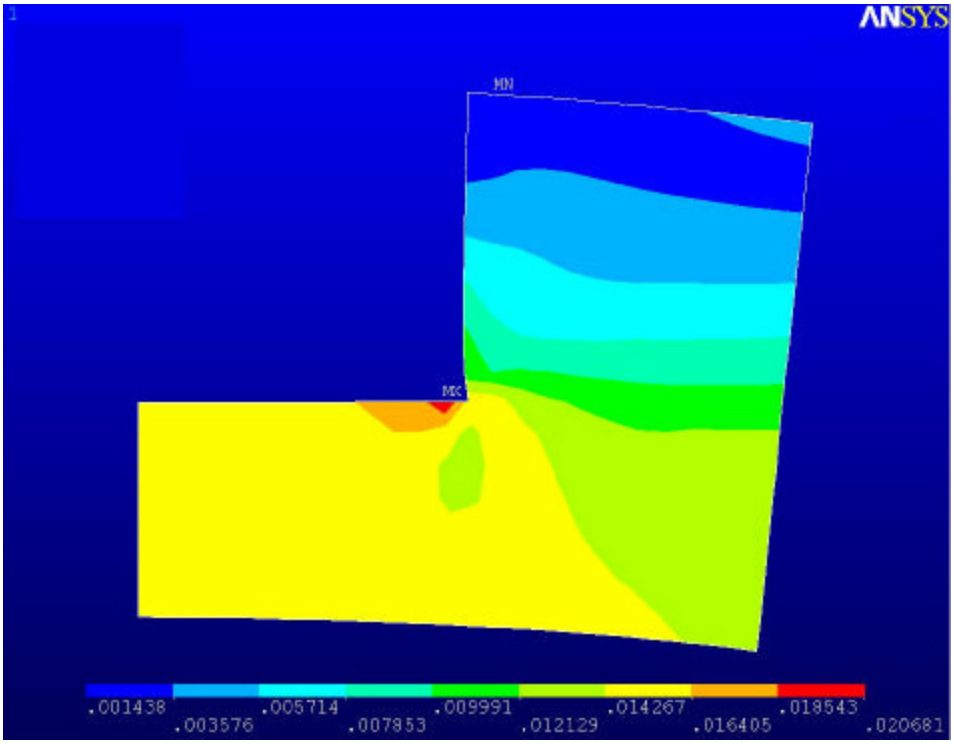

Figure 17: Total strain predicted by ANSYS around rectangular cooling channel. Highest strain (0.021) occurred at the corner of cooling channel

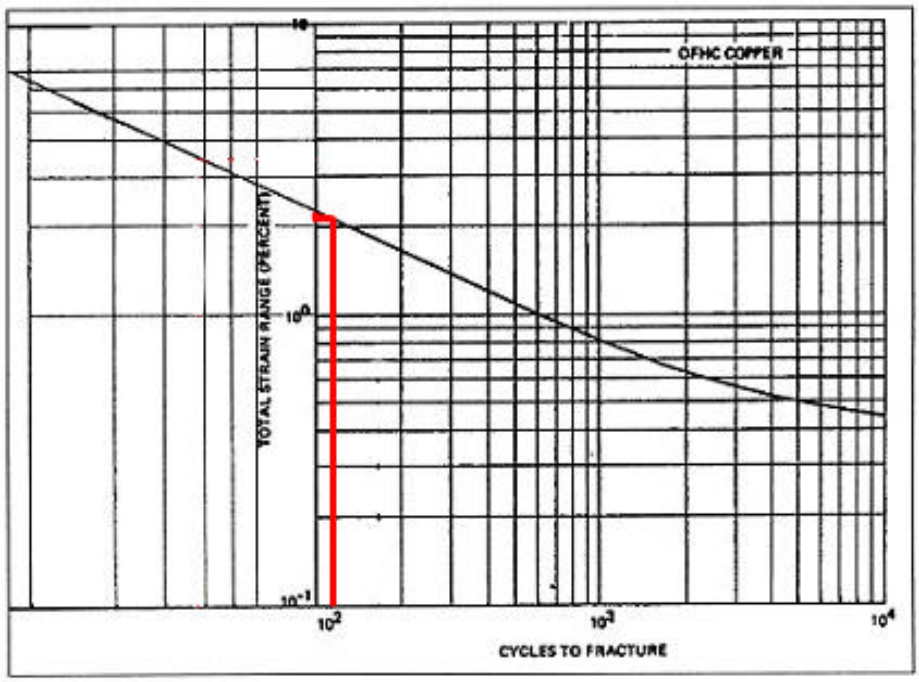

Figure 18: Strain-life curve for OHFC.[15]

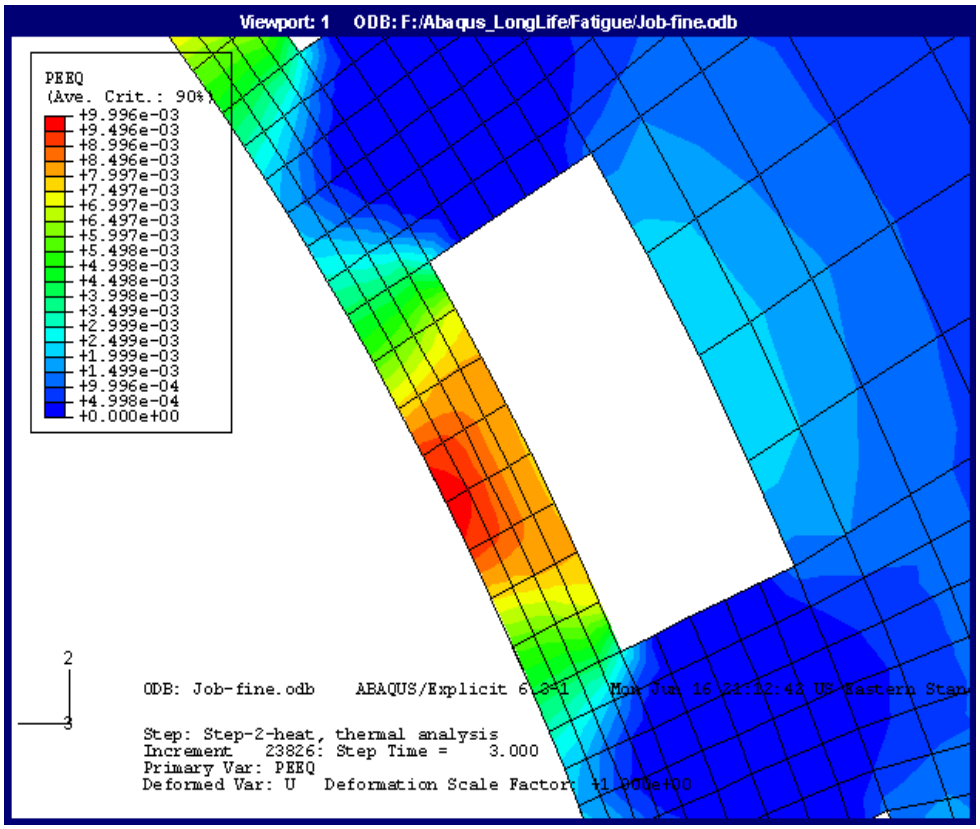

Figure 19: Equivalent plastic strain in region around rectangular cooling channel.

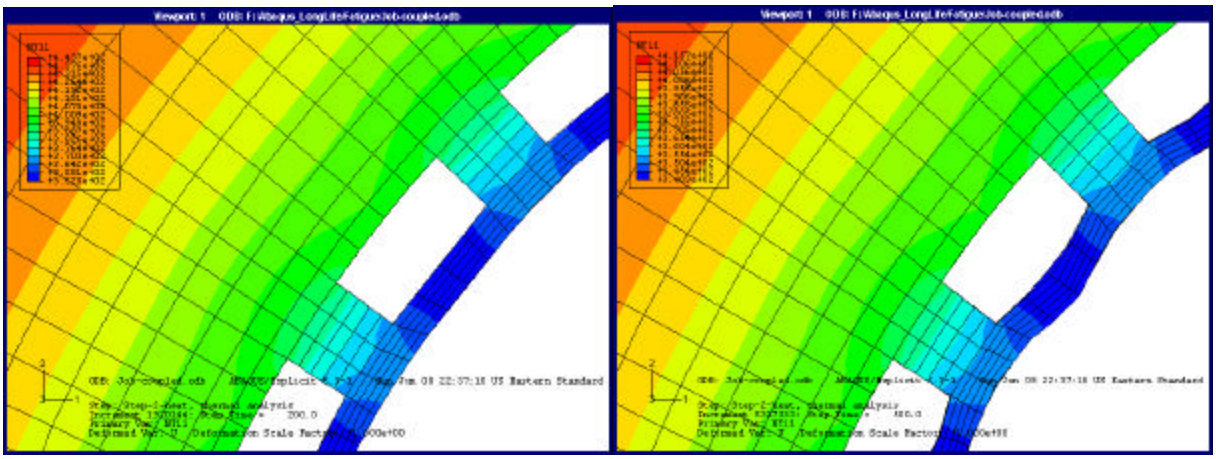

Figure 20: Deformation of channel wall at 40 (left image) and 100 cycles (right image).

From computations such as those shown in Figure 20, it was seen that deformation was predicted to begin at around 60 cycles. However, thinning was not observed in these simulations. This is due to the fact that temperature dependent experimental plastic stress strain data were implemented, instead of using visco-plastic modeling to compute fatigue deformation. Table 3 contains a summary of predicted results and measured result.

Table 3: Summary of Predicted and Measured Life

Prediction Method	Predicted Nc of cycle	Measured No. of cycl
Effective stress-strain	115	
Poroski method	51	270
Viscoplastic model	260	
FEM – ANSYS	115	
FEM – ABAQUS	320	

After the first 20 cycles, the liner had two purple spots, indicating local overheating. At the same time it was noted that several o-rings in the fuel injector were melting and causing the fuel to leak into the chamber. A copper spacer was machined and inserted between the injector and the pre-combustor to act as a block between the hot combustion gases and the fuel injector, as well as a relatively large sink. In addition to this extra spacer, Teflon O-rings were used to replace Viton O-rings, and the overheating problems were solved.

After 60 cycles, two dime-sized silver spots appeared, indicating local temperatures approaching 1400 F. At that same time, the inner surface of the liner had noticeable surface roughening. After cycle 119, the two spots had merged into one large silver spot, with considerable radial (inward) deformation. The large deformation observed was not the type of failure that was predicted; a crack was expected that

would eventually propagate and lead to a coolant flow pressure loss. A small crack did appear at the end of the 90th cycle, but no changes were noted in subsequent tests. One more set of cycles were conducted to increase the total number of cycles to 140.

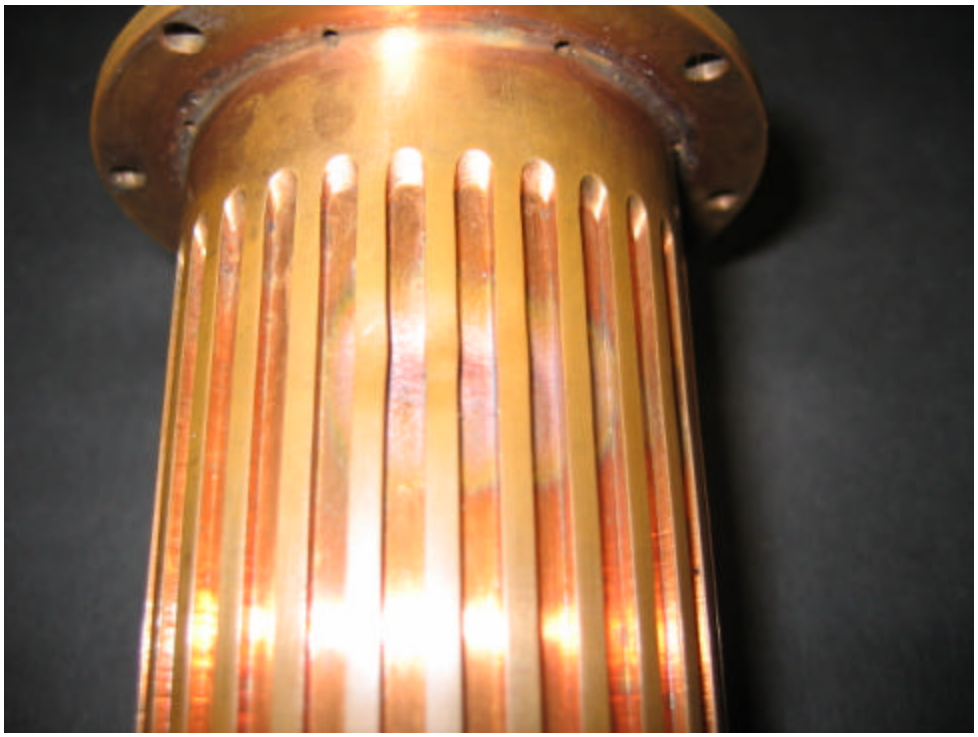

Figure 21: Liner deformation. The size of the silver-colored spot is 1.5” × 0.6” in.

A speculated failure mechanism is that the weakest portion (due to material inconsistencies or a hot spot) of the liner at the throat began to deform as normally expected by the bulging out of the coolant wall towards the interior of the chamber. However, since the liner was not fixed to the stainless steel casing, the inward bulging created a void between the copper liner and the stainless steel casing which potentially led to a lower coolant flow velocity and increased local heating. A structural analysis performed early in the design phase indicated that the free-standing liner had the strength to withstand buckling at the elevated temperature.

Another possible failure mechanism is the circumferential buckling due to difference of stress direction. Thermal loads cause compressive stress on the hot side wall and tensile stress on the coolant side. It is speculated that the weakest portion could not sustain its original shape at the high temperature and high coolant pressure. This process could have propagated very quickly during a set of 12 cycles.

CONCLUSIONS

Laboratory-scale tests and companion analyses were conducted as a first step in the development of a subscale prototype-based injector performance and life prediction methodology. These initial works were conducted under fairly benign conditions compared to the real rocket environment, but the results indicated their potential application to more severe conditions.

Measurements and predictions of the axial pressure profile in a constant area monopropellant combustor were obtained. Liquid hydrogen peroxide was injected into a flow of decomposed hydrogen peroxide. The one-dimensional pressure gradients are due to the effects of wall friction, heat transfer, and mass and enthalpy addition, with the largest effect being mass addition. Major approximations included uniform drop vaporization, infinitely fast vapor phase decomposition kinetics, and constant gas properties. The heat transfer and mass addition modeling was performed based on steady state convective and conductive heat transfer and a D^2-Law vaporization model. A comparison of calculations with and without heat transfer to the chamber walls was made and an adiabatic wall approximation was used because the difference between the two cases was small and the hot-side wall temperature could only be estimated.

Three differential pressure transducers were used to measure axial pressure profile, and a Gardon heat flux gauge was used to measure heat flux. The forward differential pressure measurement, located slightly downstream of the liquid injection point, indicated a pressure rise, which is speculated to be due to heat transfer from the gas to the injected liquid. Although the simple model presently employed approximated a constant gas temperature so the effects of heat transfer to the liquid phase and evaporative cooling was not included in the model, a simple limiting Rayleigh flow analysis indicated that a pressure rise of a similar magnitude was possible. A significant pressure drop was measured just downstream of the forward measurement. The third differential pressure drop measurement extended from the forward end of the chamber to the aft end, encompassing both of the other measurements, and was approximately equal to the sum of the other two pressure gradients that were measured. Efforts are presently underway to improve the model by using an energy balance model for drop vaporization, and the possible inclusion of finite rate vapor phase decomposition kinetics.

A number of experimental difficulties were encountered during the tests, primary among them being pressure spikes and a reduction in catalyst bed efficiency from prior tests. Although purging the instrumentation ports reduced the magnitude of the pressure spikes, it also provided an apparent hysteresis effect causing a zero-shift in the pressure differential measurement. Eventually differential pressure transducers with an extended range were used. The incomplete decomposition of the primary flow exhausting from the catalyst bed is a complication with effects that can only be approximated at this time. Efforts are underway to improve the catalyst bed, and to develop porting configurations that produce more accurate and reliable differential pressure measurements.

The measurements and analysis results show promise for their application to high pressure bipropellant combustors. This experimental/analytical approach can then be used in the analysis of subscale chambers and for preliminary design analysis. The application of this method to a high pressure oxygen/RP-1 combustor is planned for later in 2003.

In the other work reported, a small-scale rocket combustor was designed and tested to verify life prediction models for low cycle fatigue and fatigue-creep interaction. A water-cooled copper liner was tested to failure using hot gas generated by a precombustor. The liner life was about 100 cycles. Several life prediction methods were applied to predict combustor life and were compared with test results. Viscoplastic modeling showed better agreement than conventional methods in predicting the life cycle failure when both low cycle fatigue and elevated temperature loads were applied. A key improvement that could eliminate some uncertainty in the failure mechanism would be to fix the liner lands to the structural jacket. This method also shows promise for extension to more severe conditions for life prediction of full-scale components.

ACKNOWLEDGEMENTS

These works were performed under NASA grant NAG8-1856 and NAG8-1876, with technical supervision by Messrs. Huu Trinh and Robert Williams of Marshall Space Flight Center, with additional support from the School of Aeronautics and Astronautics at Purdue University. The authors wish to acknowledge the help of Professors Stephen Heister and Marc Williams of Purdue, Mr. Larry Jones of Medtherm, Messrs. Scott Meyer and Benjamin Austin of Purdue, and Ms. Madeline Chadwell of the Aerospace Sciences Laboratory of Purdue. Finally, the authors would like to acknowledge the outstanding work of the members of the student team who designed, built, and tested the combustor as part of a Design, Build, Test project at Purdue.

REFERENCES

[1]Bracco, F. V., "An Experimental-Analytical Method to Study Steady Spray Combustion", *Journal of Spacecraft*, Vol. 10, No. 6, pp. 353-354, June 1973.
[2]Burstein, S. Z., Hammer, S. S., and Agosta, V. D., "Spray Combustion Model with Droplet Breakup: Analytical and Experimental Results", *ARS Progress in Astronautics and Rocketry: Detonation and Two-Phase Flow*, edited by S. S. Penner and F. A. Williams, Vol. 6, pp. 243-267, 1961.
[3]Peschke, W. T. and Hammer, S. S., "Pressure Gradients in a Liquid Propellant Rocket Motor", *AIAA Journal*, Vol. 2, No. 8, pp. 1467-1469, August 1964.
[4]Spadaccini, L. J., "Pressure Gradients in a Variable Area Liquid-Propellant Rocket Motor", *Journal of Spacecraft*, Vol. 3, No. 7, pp.1128-1130, July 1966.
[5]Mok, J. S., Sisco, J. C., Helms, W. J., and Anderson, W. E., "Staged Thermal Decomposition and Vaporization of High Concentration Hydrogen Peroxide," Proceedings of 5th International Hydrogen Peroxide Propulsion Conference, September 2002.
[6]Shapiro, A. H., *The Dynamics and Thermodynamics of Compressible Fluid Flow*, Vol. 1, The Ronald Press Co., 1958.
[7]Fox, R. W. and McDonald, A. T., *Introduction to Fluid Mechanics*, 5th Edition, John Wiley & Sons, Inc., New York, 1998.
[8]Turns, S. R., *An Introduction to Combustion: Concepts and Applications*, 2nd Edition, McGraw-Hill Co., 2000.

[9]Ingebo, R. D. and Foster, H. H., "Drop-Size Distribution for Crosscurrent Breakup of Liquid Jets in Airstreams", NACA TN-4087, October 1957.
[10]Dai, X. and Ray, A., "Life Prediction of the Thrust Chamber Wall of a Reusable Rocket Engine," *J. of Propulsion and Power*, Vol. 11, No 6, 1995.
[11]Freed, A. D., Verrilli. M. J. "A Viscoplastic Theory Applied to Copper," NASA TM-100831, 1988.
[12]Quentmeyer, R.J., "Experimental Fatigue Life Investigation of Cylindrical Thrust Chambers," presented at the AIAA Thirteenth Propulsion Conference, Orlando, FL, July 11-13, 1977. NASA TM X-73665.
[13]Jankovsky, R.S., Arya, V. K., Kazaroff, J.M., Halford, G.R. "Structurally Compliant Rocket Engine Combustion Chamber-Experimental and Analytical Validation," NASA TP 3431, 1994.
[14]Huzel, D. K., Huang, D. H., "Modern Engineering for Design of Liquid-Propellant Rocket Engines," NASA SP-125, 1992.
[15]Esposito, J. J., and Zabora, R. F., "Thrust Chamber Life Prediction, Volume I - Mechanical and Physical Properties of High Performance Rocket Nozzle Materials," NASA CR-134806, 1975.
[16]Porowski, J.S., O'Donnell, W.J. , Badlani, M.L., Kasraie, B., and Kasper, H.J., "Simplified Design and Life Prediction of Rocket Thrust Chambers," *AIAA Journal*, Vol. 2, No. 2, March 1985.